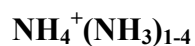


Vibrational signatures of Hydrogen bonding in the protonated ammonia clusters



Y. Yang¹, O. Kühn^{1a)}, G. Santambrogio^{2b)}, D.J. Goebbert^{3c)}, K. R. Asmis^{3d)}

¹ Institut für Chemie und Biochemie, Freie Universität Berlin, Takustr. 3, D-14195 Berlin, Germany

² Institut für Experimentalphysik, Freie Universität Berlin, Arnimallee 14, D-14195 Berlin, Germany

³ Fritz-Haber-Institut der Max-Planck-Gesellschaft, Faradayweg 4-6, D-14195 Berlin, Germany

^{a)} Present address: Institut für Physik, Universität Rostock, Universitätsplatz 3, D-18051 Rostock, Germany, Email: oliver.kuehn@uni-rostock.de.

^{b)} Present address: East Tokyo Laboratory, Genesis Research Institute, Inc., 717-86 Futamata, Ichikawa, Chiba 272-0001, Japan.

^{c)} Present address: Department of Chemistry, University of Arizona, Tucson, Arizona 85721-0041.

^{d)} Email: asmis@fhi-berlin.mpg.de.

Abstract

The gas phase vibrational spectroscopy of the protonated ammonia dimer N_2H_7^+ , a prototypical system for strong hydrogen bonding, is studied in the spectral region from 330 to 1650 cm^{-1} by combining infrared multiple photon dissociation and multidimensional quantum mechanical simulations. The fundamental transition of the antisymmetric proton stretching vibration is observed at 374 cm^{-1} and assigned on the basis of a six-dimensional model Hamiltonian, which predicts this transition at 403 cm^{-1} . Photodissociation spectra of the larger protonated ammonia clusters $\text{NH}_4^+(\text{NH}_3)_n$ with $n=2-4$ are also reported for the range from $1050-1575\text{ cm}^{-1}$. The main absorption features can be assigned within the harmonic approximation, supporting earlier evidence that hydrogen bonding in these clusters is considerably weaker than for $n=1$.

I. Introduction

Strong hydrogen bonds, characterized by large bond energies of up to 30 kcal/mol and low barriers for proton transfer, play an important role in ion solvation, proton conductivity, and proton transfer across biomembranes.¹ They are intriguing from a spectroscopic perspective, because the potential energy surface (PES) governing the displacement of the shared proton is markedly anharmonic, leading to a strong red-shift of the IR absorption, which is difficult to describe using standard quantum chemical approaches. Therefore, experimental studies on isolated model systems in the gas phase yield important benchmarks to test the accuracy of higher level computational methods.^{2,3}

For example, the complete gas phase IR spectrum of the Zundel cation $\text{H}_2\text{O}\cdots\text{H}^+\cdots\text{OH}_2$, the prototype of a strongly hydrogen bonded system, has only recently been fully understood, in particular in the region of the vibrational modes involving the shared proton (900 – 2000 cm^{-1}).^{4,5} From the theoretical point of view, the shared proton in H_5O_2^+ highlights many complications encountered in hydrogen bond research, i.e., high-level quantum chemical PESs are required for which the multidimensional quantum dynamical problem has to be solved.³ In fact, there are several reports on the spectrum of H_5O_2^+ including a reduced dimensional model,⁶ classical ab initio molecular dynamics simulations,⁷ and full-dimensional diffusion Monte Carlo and vibrational configuration interaction calculations.⁵ But only recently a full-dimensional quantum dynamical calculation based on the multiconfiguration time-dependent Hartree (MCTDH) approach has been able to assign the double peak structure to a combination of the shared proton motion and wagging torsions of the water molecules.⁸

The protonated ammonia dimer $\text{H}_3\text{N}\cdots\text{H}^+\cdots\text{NH}_3$ is isoelectronic with the Zundel cation, but presents a conceptually different scenario. In both cases the proton is equally shared between two heteroatoms, leading to D_{3d} and C_{2v} equilibrium geometries, respectively. However, the PES of the Zundel cation exhibits a single minimum at the midpoint between the oxygen atoms, while the PES of the protonated ammonia dimer has a small classical barrier (1-3 kcal/mol).⁹ In the latter case the zero point energy lifts the system over this barrier, leading to quantum mechanical symmetrization.

The experimental IR spectrum of the protonated ammonia dimer has received comparably little attention.¹⁰⁻¹² Recent IR photodissociation studies¹² were able to locate the fundamental of the antisymmetric combination of the NH_3 umbrella modes (1320 cm^{-1}) as well as the $1\cdot\nu_z+1\cdot\nu_R$ combination band, involving the antisymmetric stretching vibration of

the shared proton (ν_z) and the symmetric stretching motion of the NH_3 subunits (ν_R) motion, at 743 cm^{-1} . Further, they did find a reasonable agreement of the band positions between the infrared multiple photon dissociation (IRMPD) spectrum of the bare ion and the IR vibrational predissociation spectrum of the messenger atom tagged species $\text{N}_2\text{H}_7^+\cdot\text{Ar}$, suggesting that the IRMPD technique does yield reliable vibrational energies in this case, even though the absorption of many IR photons is required to induce fragmentation of N_2H_7^+ ($D_0 = 9440\text{ cm}^{-1}$) to form $\text{NH}_4^+ + \text{NH}_3$.¹³ However, the fundamental of the shared proton antisymmetric stretching mode ν_z remains to be identified. This transition, located at $\sim 1000\text{ cm}^{-1}$ in the Zundel cation^{4,5}, has been predicted to be significantly red-shifted from its harmonic value (1944 cm^{-1}).⁹ Anharmonic calculations based on a four-dimensional (4D) ab initio PES¹² place it at 464 cm^{-1} , i.e., significantly below the energies of the ν_z mode in other protonated homodimers² and outside the experimental observation window in Ref. ¹².

IR photodissociation studies on larger protonated ammonia clusters, $\text{NH}_4^+(\text{NH}_3)_n$, suggest that the shared proton motif is unique to the $n=1$ species, and clusters with $n>1$ exhibit a NH_4^+ core solvated by ammonia molecules.^{11,14,15} This is in contrast to protonated water clusters, in which two motifs, the Zundel (H_5O_2^+) and Eigen (H_3O^+) ion cores, persist also for larger protonated water clusters.¹⁶ Early IR photodissociation investigations^{11,17} for $n=1-10$ in the $2600-4000\text{ cm}^{-1}$ range revealed that the first solvation shell of NH_4^+ is comprised of four ammonia molecules, which exhibit nearly free internal rotation. The spectra of the larger clusters ($n>6$) converge and show similarities to that of liquid ammonia. The spectra of clusters with $n=6-9$ have also been measured in the $1045-1091\text{ cm}^{-1}$ region, where dissociation is observed due to excitation of the collective bending vibrations of NH_3 molecules in the second solvation shell.¹⁴ The issue of spectral signatures of solvation shell structures has also been addressed by a free electron laser IR study in the spectral region from $1020-1210\text{ cm}^{-1}$ for $n=5-8$ ¹⁸ and from $1070-1680\text{ cm}^{-1}$ for $n=3, 4$.¹⁵

There are several theoretical investigations of protonated ammonia clusters by Meuwly and co-workers¹⁹⁻²¹ using classical molecular dynamics together with DFT or self-consistent charge density functional tight-binding derived forces. The focus has been on proton conduction in free¹⁹ and environmentally restricted²¹ clusters, as well as on the stability and isomerization of clusters.²⁰ In terms of IR spectroscopy the predictions of Refs. ^{19,20} are based either on the harmonic approximation or on the assumption of classical nuclei. For instance, Fourier transformation of the dipole-dipole autocorrelation function along trajectories at 50 K for N_2H_7^+ gave the shared proton stretching vibration ν_z at 1610 cm^{-1} , the NH_3 umbrella vibration at 1000 cm^{-1} , and the symmetric stretching vibration ν_R at 465 cm^{-1} .²⁰

For $n > 1$ only frequencies above 2000 cm^{-1} have been reported in Ref. ²⁰. An effective one-dimensional model for the assignment of the ν_z vibration of N_2H_7^+ has been put forward by Asada et al.⁹. Their value of 707 cm^{-1} , however, is at variance with the more sophisticated 4D quantum simulation¹² which predicts this transition at 464 cm^{-1} and also has been the basis for the assignment of the $1 \cdot \nu_z + 1 \cdot \nu_R$ combination band.

In the present contribution our previous work on the protonated ammonia dimer¹² is extended in several respects. IRMPD spectra of N_2H_7^+ are presented down to 330 cm^{-1} in order to identify the ν_z fundamental. The previous 4D model of N_2H_7^+ is improved by supplementing it by the two-fold degenerate bending vibration of the shared proton. IRMPD spectra of larger protonated ammonia clusters in the $1050\text{-}1575 \text{ cm}^{-1}$ region are also presented. These systems contain considerably weaker H-bonds and an assignment of the observed spectral features is already possible within the harmonic approximation.

II. Theoretical Methods and Computational Details

A. Hamiltonian operator for N_2H_7^+

In the following we will provide a reduced dimensional model Hamiltonian for the N_2H_7^+ cation which is based on selected internal coordinates. We concentrate on that part of the spectrum which is influenced by the shared proton motion and make two simplifying assumptions: (i) the focus is on the range of experimental data ($300\text{-}1700 \text{ cm}^{-1}$) which should contain the proton stretching and bending vibrations of interest as well the low-frequency hydrogen bond mode and (ii) symmetry selection rules dominate the anharmonic couplings especially in this low-energy range. This allows us to assume that the C_3 symmetry of the N_2H_6 fragment, i.e., excluding the central proton, with respect to the N-N axis will not be broken. Further, the lengths of the N-H covalent bonds shall be fixed. These constraints leave seven coordinates as shown in

Figure 1, i.e., the shared proton stretching and bending with respect to the center of mass of the N_2H_6 fragment, z , x and y , the relative motion of the center of masses of the ammonia, R , the umbrella type motion of the two ammonia, θ_1 and θ_2 , and the rotation (torsion) of the NH_3 fragments with respect to each other, ϕ .

(

Figure 1)

To setup the Hamiltonian for this 7D model we first focus on the kinetic energy operator. In principle, there are different methods for derivation of kinetic energy operators in

non-Cartesian coordinates, see e.g. Ref.²², including constraint conditions.²³ Here, we use an approach based on the direct quantization of the classical Lagrangian. For the seven active coordinates in

Figure 1 the following kinetic energy operator can be derived under the assumptions that the total angular momentum is equal to zero and there is no kinetic energy coupling between the shared proton motion and the internal and relative motion of the NH₃ fragments (details are given in Ref.²⁴):

$$T = \frac{\hbar^2}{2\mu_p} \left(\frac{\partial^2}{\partial x^2} + \frac{\partial^2}{\partial y^2} + \frac{\partial^2}{\partial z^2} \right) - \frac{\hbar^2}{2\mu_R} \frac{1}{R^2} \frac{\partial}{\partial R} R^2 \frac{\partial}{\partial R} - \frac{\hbar^2}{2I_{rot}(\theta_1, \theta_2)} \frac{\partial^2}{\partial \phi^2} - \frac{\hbar^2}{2} \sum_{i=1,2} \frac{1}{\sin \theta_i} \frac{\partial}{\partial \theta_i} \frac{\sin \theta_i}{I_{vib}(\theta_i)} \frac{\partial}{\partial \theta_i} \quad (1)$$

The reduced masses and moments of inertia in Eq. (1) are defined as follows

$$\mu_p = \frac{2m_H(3m_H + m_N)}{7m_H + 2m_N} \quad (2a)$$

$$\mu_R = \frac{1}{2}(3m_H + m_N) \quad (2b)$$

$$I_{vib}(\theta) = I_0 \left(\cos^2 \theta + \frac{m_N}{3m_H + m_N} \sin^2 \theta \right) \quad (2c)$$

$$I_{rot}(\theta_1, \theta_2) = \frac{I_0 \sin^2 \theta_1 \sin^2 \theta_2}{\sin^2 \theta_1 + \sin^2 \theta_2} \quad (2d)$$

where $I_0 = 3m_H R_{NH}^2$ and $R_{NH} = 1.017 \text{ \AA}$ is the calculated length of the N-H covalent bonds of the NH₃ fragments. Using these coordinates the wave function will be normalized by the Euclidean volume element $d\tau = R^2 \sin \theta_1 \sin \theta_2 dx dy dz dR d\theta_1 d\theta_2 d\phi$.

The torsion angle ϕ of the two NH₃ fragments can be separated from the other six variables if the potential energy does not depend on it. We have confirmed that the ab initio PES depends only very weakly on this angle (the barrier is as low as 12 cm⁻¹). Moreover, there is a clear separation between the rotational and vibrational excitation energies. Thus, we can separate this torsion and replace the operator $-\partial^2/\partial\phi^2$ by its expectation value, say, K^2 . For the numerical implementation below it is more convenient to use another set of coordinates and an appropriately modified wave function which simplifies both the kinetic energy operator and the normalization volume element. Assuming $K^2=0$ we will use the following six-dimensional (6D) kinetic energy operator

$$T = \frac{\hbar^2}{2\mu_p} \left(\frac{\partial^2}{\partial x^2} + \frac{\partial^2}{\partial y^2} + \frac{\partial^2}{\partial z^2} \right) - \frac{\hbar^2}{2\mu_R} \frac{\partial^2}{\partial R^2} - \frac{\hbar^2}{2I_0} \sum_{i=1,2} \frac{\partial}{\partial u_i} g(u_i) \frac{\partial}{\partial u_i} \quad (3)$$

with the volume element $d\tau = dx dy dz dR du_1 du_2$ and the definitions $u_i = \cos u_i$ and

$$g(u) = (1 - u^2)(3m_H + m_N) / (3m_H u^2 + m_N).$$

Next we specify the construction of the respective 6D PES. Here, we make use of the cumulative expansion in terms of different correlation orders²⁵

$$V(\mathbf{Q}) = \sum_i V^{(1)}(Q_i) + \sum_{i<j} V^{(2)}(Q_i, Q_j) + \sum_{i<j<k} V^{(3)}(Q_i, Q_j, Q_k) + \mathbf{K} \quad (4)$$

where \mathbf{Q} is a vector comprising the six model coordinates and $V^{(n)}$ is the n -th correlation potential which is defined by the subtraction of all lower order correlations and the uncorrelated one-dimensional potential $V^{(1)}(Q_i)$ from the n -dimensional PES. Our final expansion includes all two-mode correlations as well as those three-mode correlations concerning the z coordinate except $V^{(3)}(z, \theta_1, \theta_2)$ and $V^{(3)}(z, R, \theta_{1/2})$ which are assumed to be negligible as compared to the contributions involving two proton coordinates like $V^{(3)}(x, z, R)$. The 6D dipole moment surface is constructed in the same spirit, that is, for each of the three vector components we employed the following approximation:

$$\mu(\mathbf{Q}) = \sum_i \mu^{(1)}(Q_i) + \sum_{i<j} \mu^{(2)}(Q_i, Q_j). \quad (5)$$

B. Numerical Implementation

PES and dipole moment surface are calculated using the MP2 method with the aug-cc-pVTZ and cc-pVTZ basis set for N and H, respectively, using Gaussian 03.²⁶ In total about 10.000 points have been calculated and applying symmetry we obtain more than 90.000 points spanning the energy range up to 10.000 cm^{-1} . This PES has been fit subsequently to a polynomial of up to 10th order.

For the solution of the nuclear Schrödinger equation we have used the MCTDH approach^{27,28} as implemented in the Heidelberg program package.²⁹ The wave function is represented as a superposition of Hartree products composed of single particle functions (SPFs) for either individual or combined degrees of freedom. The single particle functions themselves are defined on a primitive grid using a harmonic oscillator discrete variable representation (DVR). The details of the basis set for the MCTDH calculation are collected in Table 1.

(Table 1)

We have calculated low lying excited state by the improved relaxation method as detailed in Ref. ³⁰. The MCTDH equations of motion have been solved using a 6th order Bulirsch-Stoer method for the SPFs and a 16th order Davidson algorithm for the coefficient vector.²⁷ The assignment below will be based on variables quite close to certain normal modes, i.e.,

$$\langle zR\theta_s\theta_a xy | mnkl ij \rangle = \Psi_{mnkl ij} (z, R, \theta_s, \theta_a, x, y) \quad (6)$$

where $m, n, k, l, i,$ and j are the quantum numbers associated to the coordinates $z, R, \theta_s = (\theta_1 + \theta_2) / 2, \theta_a = (\theta_1 - \theta_2) / 2, x,$ and $y,$ respectively.

C. Larger Clusters: $\text{NH}_4^+(\text{NH}_3)_{2-4}$

In principle it would be straightforward to apply the method outlined above to larger clusters as well. It turns out, however, that the hydrogen bonding in N_2H_7^+ is exceptional insofar as it is particularly strong compared to $\text{NH}_4^+(\text{NH}_3)_{2-4}$. Consequently, the PES for the larger clusters is considerably less anharmonic. We have calculated the equilibrium geometries of these clusters using the MP2/6-311++G(d,p) level of theory.

(

Figure 2)

To address the degree of anharmonicity the potential curve along one of the hydrogen-bonded N-H stretching coordinates has been determined within the otherwise frozen structures. The results in

Figure 2 show that upon increasing n the potential becomes less anharmonic. For $n=2$ it still shows some double minimum topology, although the proton transfer minimum is considerably less stable. Notice that the actual well depth depends on the level of quantum chemistry, for instance, it increases slightly if the larger basis set of the previous section is used. For $n=3, 4$ there is no stable proton transfer minimum at all. Based on the results in

Figure 2 we will restrict our discussion to the harmonic limit, which proves to be sufficient for analyzing the size dependence of the experimental spectra. However, one should note that a more quantitative discussion would require to take into account the anharmonicity, especially for $n=2$.

III. Experimental Setup

Most of the experiments were carried out on a previously described tandem mass spectrometer-ion trap system.³² $\text{NH}_4^+(\text{NH}_3)_n$ clusters are produced by crossing a supersonic expansion of $\sim 0.2\%$ ammonia in Ar with a 300 μA , 1keV electron beam. The supersonic expansion is generated by expanding the gas mixture with a backing pressure of 6 bar into

vacuum through a 20 μm orifice. The cations pass through a 2 mm skimmer, are thermalized to room temperature by collision with He buffer gas in a radio frequency (RF) ion guide, then mass-selected by a quadrupole mass spectrometer. Subsequently, the mass-selected ions are collected in a He filled linear RF hexadecapole ion trap, which is connected to a closed-cycle helium cryostat and kept at a temperature of <20 K. Collisions with the He buffer gas (~ 0.03 mbar) slow the ions and cool them to the ambient temperature.

IR photodissociation spectra are obtained by photoexcitation of the trapped ions with pulsed radiation from the “Free Electron Laser for Infrared eXperiments” FELIX.³³ Immediately after irradiation, the trap is emptied and the ions are mass-selectively monitored using a second quadrupole mass spectrometer. Photodissociation manifests itself as a depletion of the parent ion signal and production of charged fragments. The mass selected ion yield of parents and fragments is recorded as a function of FELIX wavelength. This data acquisition cycle is repeated multiple times for every wavelength step.

The IRMPD spectra of N_2H_7^+ below 600 cm^{-1} were recorded using a second tandem mass spectrometer. Its operation is very similar to the spectrometer described in Ref. ³¹, in particular similar ion production and trapping settings were used, but it makes use of a conceptually different ion extraction / mass analyzing strategy. The hexadecapole ion trap and second quadrupole mass filter are replaced by a ring electrode trap and time-of-flight mass spectrometer, which more efficiently combines continuous ion production schemes with pulsed laser experiments on the thermalized ions at defined temperature. A more detailed description of this instrument will be part of a separate publication.

IV. Results and Discussion

A. N_2H_7^+ : PES and Vibrational Ground State

A two-dimensional cut of the 6D PES along the proton transfer coordinate z and the N-N distance R with other coordinates fixed at transition state, i.e., $\theta_1 = \theta_2 = 111.7^\circ$ and $x=y=0$, is shown in

Figure 3a. The PES exhibits two minima at $R=2.83\text{ \AA}$, which correspond to two equivalent C_{3v} configurations in which the central proton is not equally shared ($z=\pm 0.24\text{ \AA}$). These minima are connected via a D_{3h} transition state at a slightly compressed N-N distance ($R=2.73\text{ \AA}$). The barrier height for the fully relaxed surface is 267 cm^{-1} , which increase to 353 cm^{-1} when the CCSD(T)/aug-cc-pVTZ energies (at the MP2/ aug-cc-pVTZ geometries) are used. Independent on the level of quantum chemistry (see also Ref. ⁹) the barrier is rather low, in particular, it lies below the zero point energy.

(

Figure 3)

Calculation of the 6D vibrational ground state yields the reduced probability density shown in

Figure 3b. The most notable feature is that this function has a single maximum at the symmetric D_{3h} configuration. In other words, despite the sizable barrier height, the correlated quantum mechanical zero point energy is large enough to *symmetrize* the hydrogen bond. This feature has been discussed previously in the context of the IR spectroscopy in the 2600-4000 cm^{-1} range in Ref. ¹¹; see also one-dimensional model in Ref. ⁹ and our previous results in Ref. ¹².

(Table 2)

B. N_2H_7^+ : Vibrational Excited States

Vibrational excitation energies and linear absorption intensities below 1600 cm^{-1} of the 6D model calculations are listed in Table 2. Excitation energies corresponding to the fundamentals of the symmetric stretching ν_R , antisymmetric stretching ν_z , symmetric umbrella (ν_{0s}), antisymmetric umbrella (ν_{0a}), and the doubly degenerate proton bending (ν_{xy}) vibrations are calculated at 403, 409, 1336, 1369, and 1545 cm^{-1} , respectively. Notice that compared to the harmonic prediction the ν_z frequency is significantly red-shifted by about 1500 cm^{-1} . The effective one-dimensional calculation in Ref. ⁹ (707 cm^{-1}) only captures part of this anharmonicity. In comparison to the result of 4D model calculations (464 cm^{-1}) reported in Ref. ¹² the inclusion of the two bending vibrations of the shared proton in the present 6D model causes an additional red shift of this transition by 55 cm^{-1} .

Excitation of the ν_z fundamental is predicted to be the most intense transition, which is expected, because the displacement of the shared proton along the N-N atom axis produces a large dipole oscillation. Exclusive excitation of the ν_R and ν_{0s} modes, on the other hand, is dipole forbidden, which can be derived from the symmetry of the dipole moment operator:

$$\mu(-z, R, -\theta_a, \theta_s, -x, -y) = -\mu(z, R, \theta_a, \theta_s, x, y). \quad (7b)$$

However, combined excitation of the symmetric and antisymmetric stretching modes is dipole allowed, whenever an odd number of quanta of the antisymmetric stretching mode is involved. Indeed, excited states, corresponding to the 1+1 (713 cm^{-1}), 1+2 (1002 cm^{-1}) and 1+3 (1306 cm^{-1}) combinations of the $\nu_z + \nu_R$ modes, are predicted to have non-zero intensities (see Table 2).

(

Figure 4)

The reduced density of the $|110000\rangle$, $|000100\rangle$, $|100000\rangle$, and $|000010\rangle$ wave functions is shown in

Figure 4. It is interesting to note that the probability density corresponding to the shared proton stretching motion ($|100000\rangle$) is localized in the two well regions in contrast to the ground state wave function shown in

Figure 3. The antisymmetric combination character of the ν_{0a} mode is obvious from the reduced density in

Figure 4 ($|000100\rangle$).

(

Figure 5)

C. $N_2H_7^+$: Experimental IR Spectra

IRMPD spectra of trapped and cooled $N_2H_7^+$ in the 330-1650 region are shown in Figure 5. The more recent measurements at longer wavelengths reveal a new, intense absorption feature below 500 cm^{-1} ; a $\sim 60\text{ cm}^{-1}$ broad band peaking at 374 cm^{-1} and exhibiting additional structure on its high-energy tail. Based on our 6D model calculations (see Table 2 and stick spectrum in

Figure 5) it seems reasonable to assign this band, and in particular the maximum at 374 cm^{-1} , to the fundamental of the ν_z mode. The only other IR active mode in this frequency range, albeit of comparably weak intensity compared to the IR active modes above 1250 cm^{-1} (see Figure 2d in Ref. ¹²), is the doubly degenerate wagging vibration of e_u symmetry, calculated at 418 cm^{-1} within the harmonic approximation. The presence of a second IR active transition is supported by the observation of a relative maximum at 409 cm^{-1} (labeled a' in Figure 6). However, peak a' together with another, weaker feature at 444 cm^{-1} (a'') may also suggest a progression in a low frequency mode ($\sim 35\text{ cm}^{-1}$), indicating efficient coupling of the ν_z mode to a low frequency wagging mode, which is calculated at 34 cm^{-1} within the harmonic approximation. These wagging modes were not included in the 6D model and therefore an assignment of features a' and a'' will have to wait until higher dimensionality calculations become available.

The spectrum shown in the right part of

Figure 5 has been previously reported.¹² Briefly, bands A (743 cm^{-1}), C (1097 cm^{-1}), and Band D (1325 cm^{-1}) are the $1\cdot\nu_z+1\cdot\nu_R$ and $1\cdot\nu_z+2\cdot\nu_R$ combination bands and the

fundamental of the ν_{0a} mode, respectively. The present 6D model places these transitions at 713, 1002 and 1336 cm^{-1} . While the agreement for the ν_{0a} mode is slightly improved compared to the 4D model (1354 cm^{-1}), it is less good for the combination bands. Bands F (1451 cm^{-1}) and G (1545 cm^{-1}) were tentatively attributed to the $1\cdot\nu_z+3\cdot\nu_R$ combination band and the fundamental of the ν_{xy} mode, respectively. The present 6D model (1542 cm^{-1}) confirms the assignment of band G to the ν_{xy} mode, while it draws into question the previous assignment of the 1+3 combination band (1306 cm^{-1}).

In summary, the fundamental of the shared proton antisymmetric stretching mode in N_2H_7^+ has been observed for the first time. In comparison to the previously reported 4D calculations, the present 6D model yields an improved description of this transition, as well as of the fundamentals of the antisymmetric umbrella and the shared proton bending motion. On the other hand, the description of the combined excitation of the antisymmetric and symmetric shared proton stretching modes deteriorates, spotlighting the limitations of the 6D model. Smaller absorption features observed in the IRMPD spectra suggest that the wagging modes may efficiently couple to the stretching motion. Thus, these modes should be included in an improved model, at least until a full dimensional description of the vibrational spectroscopy of N_2H_7^+ becomes possible.

C. Larger Protonated Ammonia Clusters: $\text{NH}_4^+(\text{NH}_3)_{2-4}$

The experimental IRMPD spectra of cooled $\text{NH}_4^+(\text{NH}_3)_n$ clusters with $n=2-4$ are shown in Figure 6 (left panel). Loss of a single ammonia molecule is the main dissociation channel for all clusters studied here. The dominant absorption peak found between 1100 and 1200 cm^{-1} is progressively red-shifted with increasing cluster size. The second most intense feature is a group of bands centered around 1500 cm^{-1} whose overall width decreases with cluster size. Our IRMPD spectra are in satisfactory agreement with the photodissociation spectra measured recently by Tono et al.¹⁵ for $n=3$ and $n=4$. These latter spectra were measured for ions with an internal temperature >200 K under single photon absorption conditions.

(

Figure 6)

In order to assign the main spectral features we performed MP2 calculations. Simulated linear absorption spectra are shown on right side of

Figure 6. The most intense absorption bands, found at 1182, 1151 and 1135 cm^{-1} in the IRMPD spectra of $n=2-4$, respectively, are assigned to the excitation of the collective ν_2 bending modes of the NH_3 molecules. The red shift of the ammonia ν_2 mode with increasing

cluster size is due to a weakening of the hydrogen bonds, also reflected in the increase of the N-N distances with cluster size: 2.82 Å ($n=2$), 2.9 Å ($n=3$), and 2.96 Å ($n=4$). For comparison, the ν_2 mode continuous to be red-shifted in larger protonated ammonia clusters¹⁴ from 1080 cm^{-1} in $n=6$ to below 1060 cm^{-1} in $n=9$ and ultimately appears at 950 cm^{-1} in the isolated ammonia molecule.³⁵

The change in the overall widths of the groups of bands around 1500 cm^{-1} is qualitatively reproduced by the MP2 calculations. As noted before we do not consider the harmonic approximation to yield sufficiently accurate results and therefore will not assign individual peaks in the spectrum. However, in view of the previous work by Tono et al.¹⁵ (for $n=3,4$; spectra included in Fig. 6) and by Schwarz³⁶ as well as Lee and coworkers¹¹ for $n=4$ these bands should be dominated by the fundamental transitions of the NH_4^+ ν_4 mode as well as of the collective asymmetric NH_3 ν_4 -bending vibration. Note, however, that the photodissociation studies of Tono et al.¹⁵ find evidence for these transitions at 1625 cm^{-1} ($n=3$) and 1599 cm^{-1} ($n=4$), that is, outside our measurement window.

V. Summary

In summary we have given a combined experimental and theoretical study of the gas phase infrared absorption spectra of protonated ammonia clusters $\text{NH}_4^+(\text{NH}_3)_n$ with $n=1-4$. The most interesting case is certainly the protonated ammonia dimer, N_2H_7^+ , whose strong hydrogen bond has been characterized by its spectral features in the region from 330 to 1650 cm^{-1} . For the first time we report the assignment of the fundamental transition of the antisymmetric proton stretching vibration which is observed at 374 cm^{-1} . The enormous red-shift as compared to a free NH stretching vibration clearly stands for the substantial modification of the potential energy surface upon strong hydrogen bonding which can hardly be described by few dimensional models. While the performance of the present 6D model is rather good for some fundamental and combination transitions, the assignment of the full spectrum in this range calls for an extension to include at least wagging vibration of the terminal NH_3 groups. In comparison the larger clusters $\text{NH}_4^+(\text{NH}_3)_n$ ($n=2-4$) behave more predictable and the gross features in the reported range from 1050-1575 cm^{-1} can be assigned within the harmonic approximation. This gives evidence that hydrogen bonding in these clusters is considerably weaker than for $n=1$.

Acknowledgements

This work has been supported by the Deutsche Forschungsgemeinschaft through the Graduate Research School 788. We gratefully acknowledge the support of the Stichting voor Fundamenteel Onderzoek der Materie (FOM) in providing the required beam time on FELIX and highly appreciate the skillful assistance of the FELIX staff.

References

- ¹ D. Marx, *ChemPhysChem* **7**, 1848 (2006).
- ² K. R. Asmis, D. M. Neumark, and J. M. Bowman, in *Hydrogen-Transfer Reactions: Physical and Chemical Aspects*, edited by J. T. Hynes, J. P. Klinman, H.-H. Limbach, and R. L. Schowen (Wiley-VCH, Weinheim, Germany, 2007), Vol. 1, pp. 53; J. R. Roscioli, L. R. McCunn, and M. A. Johnson, *Science* **249**, 249 (2007).
- ³ K. Giese, M. Petković, H. Naundorf, and O. Kühn, *Phys. Rep.* **430**, 211 (2006).
- ⁴ K. R. Asmis, N. L. Pivonka, G. Santambrogio, M. Brummer, C. Kaposta, D. M. Neumark, and L. Woste, *Science* **299**, 1375 (2003).
- ⁵ N. I. Hammer, E. G. Diken, J. R. Roscioli, M. A. Johnson, E. M. Myshakin, K. D. Jordan, A. B. McCoy, X. Huang, J. M. Bowman, and S. Carter, *J. Chem. Phys.* **122**, 244301 (2005).
- ⁶ M. V. Vener, O. Kühn, and J. Sauer, *J. Chem. Phys.* **114**, 240 (2001).
- ⁷ J. Sauer and J. Döbler, *ChemPhysChem* **6**, 1706 (2005).
- ⁸ O. Vendrell, F. Gatti, D. Lauvergnat, and H. D. Meyer, *J. Chem. Phys.* **127**, 184302 (2007); O. Vendrell, F. Gatti, and H.-D. Meyer, *Angew. Chem. Int. Ed.* **46**, 6918 (2007); O. Vendrell, F. Gatti, and H. D. Meyer, *J. Chem. Phys.* **127**, 184303 (2007); O. Vendrell and H. D. Meyer, *Phys. Chem. Chem. Phys.* **10**, 4692 (2008).
- ⁹ T. Asada, H. Haraguchi, and K. Kitaura, *J. Phys. Chem. A* **105**, 7423 (2001).
- ¹⁰ H. A. Schwarz, *J. Chem. Phys.* **72**, 284 (1980).
- ¹¹ J. M. Price, M. W. Crofton, and Y. T. Lee, *J. Phys. Chem.* **95**, 2182 (1991).
- ¹² K. R. Asmis, Y. Yang, G. Santambrogio, M. Brümmer, J. R. Roscioli, L. R. McCunn, M. A. Johnson, and O. Kühn, *Angew. Chem. Int. Ed.* **46**, 8691 (2007).
- ¹³ S. K. Sears and P. Kebarle, *J. Phys. Chem.* **72**, 742 (1968).
- ¹⁴ M. Ichihashi, J. Yamabe, K. Murai, S. Nonose, K. Hirao, and T. Kondow, *J. Phys. Chem.* **100**, 10050 (1996).

- 15 K. Tono, K. Fukazawa, M. Tada, N. Fukushima, and K. Tsukiyama, *Chem. Phys. Lett.* **442**, 206 (2007).
- 16 J. M. Headrick, E. G. Diken, R. S. Walters, N. I. Hammer, R. A. Christie, J. Cui, E. M. Myshakin, M. A. Duncan, M. A. Johnson, and K. D. Jordan, *Science* **308**, 1765 (2005).
- 17 J. M. Price, M. W. Crofton, and Y. T. Lee, *J. Chem. Phys.* **91**, 2749 (1989).
- 18 K. Tono, K. Bito, H. Kondoh, T. Ohta, and K. Tsukiyama, *J. Chem. Phys.* **125**, 224305 (2006).
- 19 M. Meuwly and M. Karplus, *J. Chem. Phys.* **116**, 2572 (2002).
- 20 A. Fouqueau and M. Meuwly, *J. Chem. Phys.* **123**, 244308 (2005).
- 21 V. Zoete and M. Meuwly, *J. Chem. Phys.* **120**, 7085 (2004).
- 22 C. Iung, F. Gatti, A. Viel, and X. Chapusiat, *Phys. Chem. Chem. Phys.* **1**, 3377 (1999); E. B. Wilson, J. C. Decius, and P. C. Cross, *Molecular Vibrations*. (Dover, New York, 1955).
- 23 A. Nauts and X. Chapusiat, *Chem. Phys. Lett.* **136**, 164 (1987).
- 24 Y. Yang and O. Kühn, submitted.
- 25 S. Carter, S. J. Culik, and J. M. Bowman, *J. Chem. Phys.* **107** (24), 10458 (1997).
- 26 M. J. Frisch, G. W. Trucks, H. B. Schlegel, G. E. Scuseria, M. A. Robb, J. R. Cheeseman, J. Montgomery, J. A., T. Vreven, K. N. Kudin, J. C. Burant, J. M. Millam, S. S. Iyengar, J. Tomasi, V. Barone, B. Mennucci, M. Cossi, G. Scalmani, N. Rega, G. A. Petersson, H. Nakatsuji, M. Hada, M. Ehara, K. Toyota, R. Fukuda, J. Hasegawa, M. Ishida, T. Nakajima, Y. Honda, O. Kitao, H. Nakai, M. Klene, X. Li, J. E. Knox, H. P. Hratchian, J. B. Cross, V. Bakken, C. Adamo, J. Jaramillo, R. Gomperts, R. E. Stratmann, O. Yazyev, A. J. Austin, R. Cammi, C. Pomelli, J. W. Ochterski, P. Y. Ayala, K. Morokuma, G. A. Voth, P. Salvador, J. J. Dannenberg, V. G. Zakrzewski, S. Dapprich, A. D. Daniels, M. C. Strain, O. Farkas, D. K. Malick, A. D. Rabuck, K. Raghavachari, J. B. Foresman, J. V. Ortiz, Q. Cui, A. G. Baboul, S. Clifford, J. Cioslowski, B. B. Stefanov, G. Liu, A. Liashenko, P. Piskorz, I. Komaromi, R. L. Martin, D. J. Fox, T. Keith, M. A. Al-Laham, C. Y. Peng, A. Nanayakkara, M. Challacombe, P. M. W. Gill, B. Johnson, W. Chen, M. W. Wong, C. Gonzalez, and J. A. Pople, *Gaussian 03, Revision B.04* (Gaussian Inc., Wallingford, CT, 2004).
- 27 M. H. Beck, A. Jäckle, H.-D. Meyer, and G. A. Worth, *Phys. Rep.* **324**, 1 (2000).
- 28 H. D. Meyer and G. A. Worth, *Theor. Chem. Acc.* **109**, 251 (2003).

- ²⁹ G. A. Worth, M. Beck, A. Jäckle, and H.-D. Meyer, The MCTDH Package (University of Heidelberg, Heidelberg, 2003).
- ³⁰ H. D. Meyer, F. Le Quéré, C. Léonard, and F. Gatti, *Chem. Phys.* **329**, 179 (2006).
- ³¹ K. R. Asmis, M. Brümmer, C. Kaposta, G. Santambrogio, G. von Helden, G. Meijer, K. Rademann, and L. Wöste, *Phys. Chem. Chem. Phys.* **4**, 1101 (2002).

Figure Captions

Figure 1: Definition of the seven active coordinates of the reduced N_2H_7^+ model. Note that compared to our previous model¹² we have incorporated the bending vibrations of the shared proton.

Figure 2: One dimensional MP2/6-311+G(d,p) (solid lines) and MP2/aug-cc-pVTZ (dashed line) potential energy curves of $\text{NH}_4^+(\text{NH}_3)_n$ cations along an $\text{N}\cdots\text{H}\cdots\text{N}$ proton transfer coordinate connecting the N-atoms of the NH_4^+ core and of one of the NH_3 ligands.

Figure 3: (a) Two-dimensional cut of the 6D MP2/aug-cc-pVTZ PES. (b) Ground state reduced probability density (see text). PES contours run from -150 to 1550 cm^{-1} in steps of 100 cm^{-1} .

Figure 4: Selected low energy wave functions (reduced densities) as indicated by the labels $|mnklj\rangle$, cf. Eq. (6), of the N_2H_7^+ cation. PES contour values: (left column, see Figure 3), upper right: 200-3000 cm^{-1} in steps of 200 cm^{-1} , lower right: 200-5000 cm^{-1} in steps of 300 cm^{-1} .

Figure 5: Experimental IRMPD spectra (top) and calculated linear absorption spectrum (bottom) of N_2H_7 in the region from 350 to 1650 cm^{-1} . The IRMPD spectra (the right trace is from Ref. ¹²) were measured by monitoring the NH_4^+ ion fragment as a function of irradiation wavelength. Letters index the prominent peaks for reference in Table 2. The black bars reflect the dipole-allowed transition energies and intensities from the 6D model calculations (see Table 2).

Figure 6: Experimental IRMPD spectra (left) and simulated linear absorption spectra (right) of $\text{NH}_4^+(\text{NH}_3)_{2,4}$ in the region from 1050 to 1575 cm^{-1} . Two experimental spectra are shown for $n=3, 4$: (a) present study, (b) spectrum taken from Ref. 15. The simulated spectra were derived from MP2/6-311+G(d,p) harmonic frequencies (scaled by 0.95) and intensities and convoluted using a Gaussian line function with a width of 15 cm^{-1} (FWHM).

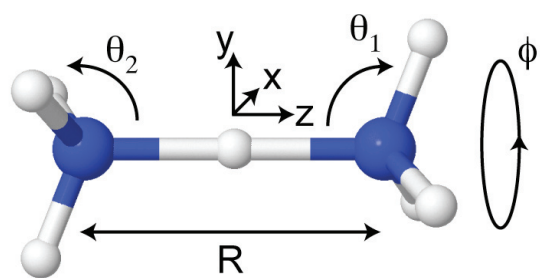
Table 1. MCTDH parameters for solving the Schrödinger equation (lengths in Å). N_{DVR} : number of DVR points; N_{SPF} : number of SPFs (Note that u_s and u_a as well as x and y have been treated as combined modes.). The largest natural orbital population has been 0.01%.

Mode	z	R	u_s	u_a	x	y
min. grid	-0.58	2.20	-0.61	-0.61	-0.53	-0.53
max grid	0.58	3.26	0.13	0.13	0.53	0.53
N_{DVR}	59	39	39	39	39	39
N_{SPF}	9	8	9		3	

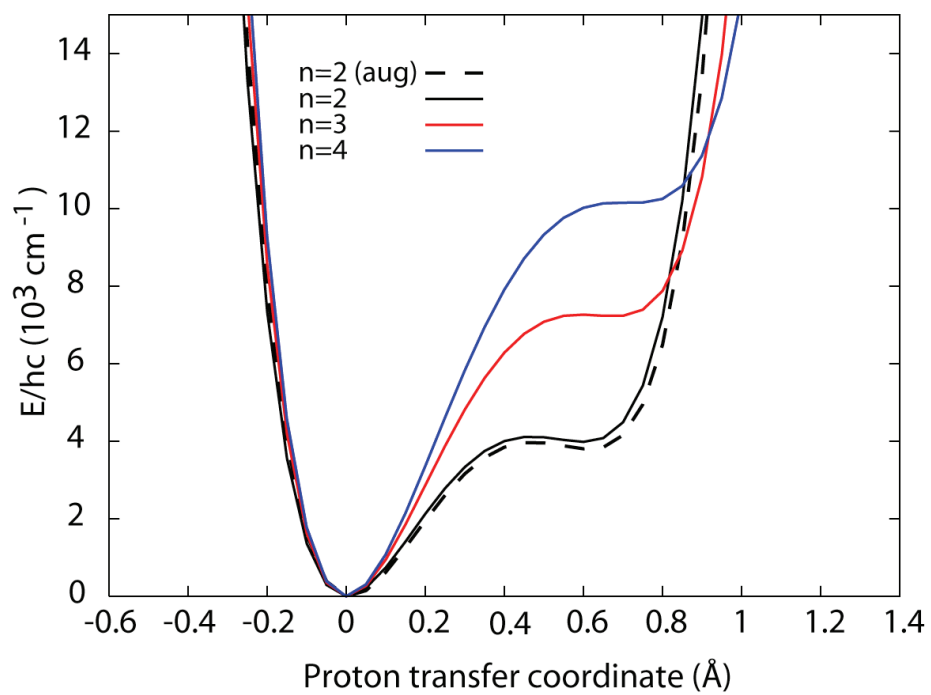
Table 2. Calculated excitation energies (in cm^{-1}), relative IR intensities (in parentheses) and their assignment from the anharmonic 6D model for N_2H_7^+ below 1600 cm^{-1} . Excitation energies from the previously reported anharmonic 4D model¹², harmonic MP2/aug-cc-pVTZ calculations (unscaled) at the C_{3v} minimum (Min_{harm}) and D_{3h} transition state (TS_{harm}) geometries, as well as experimental IRMPD band positions (Exp) are also listed. The states are labeled according to Eq. (6).

State	Excitation Energy (cm^{-1})					Assignment
	6D	4D	TS_{harm}	Min_{harm}	Exp	
$ 010000\rangle$	403 (0.00)	421	565	313*		$1\nu_R$
$ 100000\rangle$	409 (1.00)	464	843i	1944	374	$1\nu_z$
$ 020000\rangle$	701 (0.00)	729				$2\nu_R$
$ 110000\rangle$	713 (0.37)	765			743	$1\nu_z + 1\nu_R$
$ 030000\rangle$	981 (0.00)	1030				$3\nu_R$
$ 120000\rangle$	1002 (0.12)	1091			1097	$1\nu_z + 2\nu_R$
$ 130000\rangle$	1306 (???)	1485			1451	$1\nu_z + 3\nu_R$
$ 000100\rangle$	1336 (0.48)	1354	1362	1380*	1325	$1\nu_{\theta a}$
$ 001000\rangle$	1369 (0.00)	1348	1342	1264*		$1\nu_{\theta s}$
$ 000010\rangle$	1542 (0.46)		1777	1777	1545	$1\nu_{xy}$

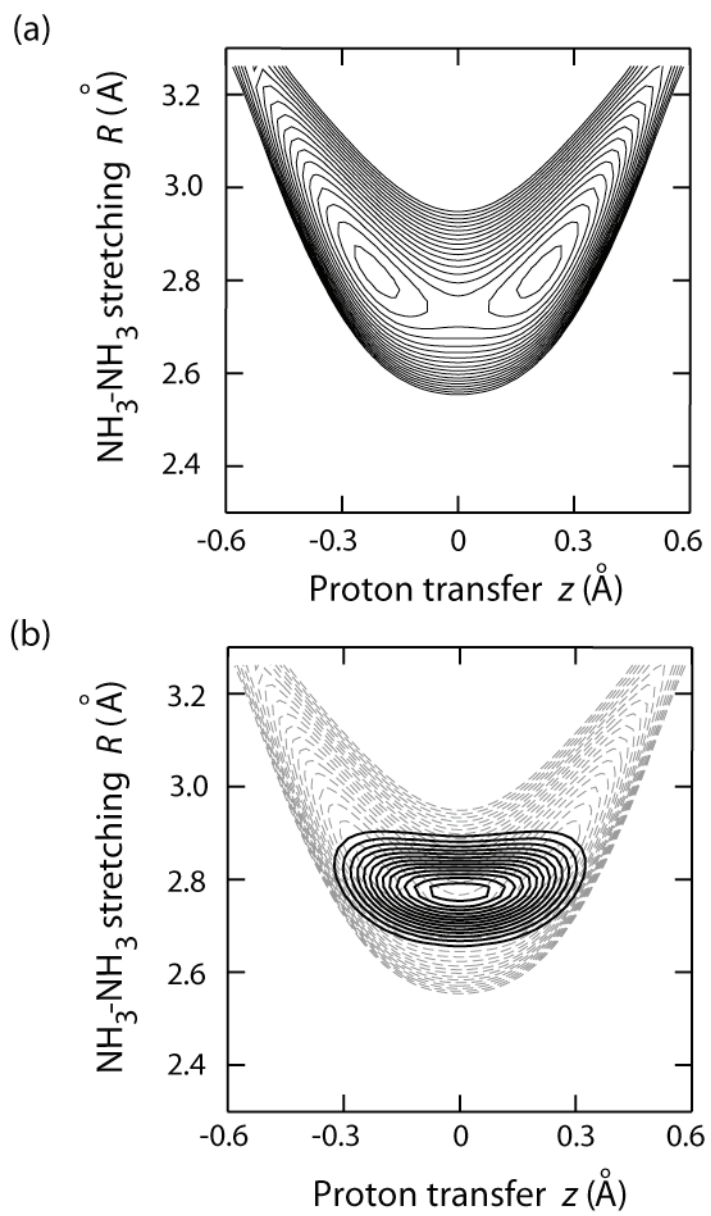
* These modes are not exactly the same as the assignments.



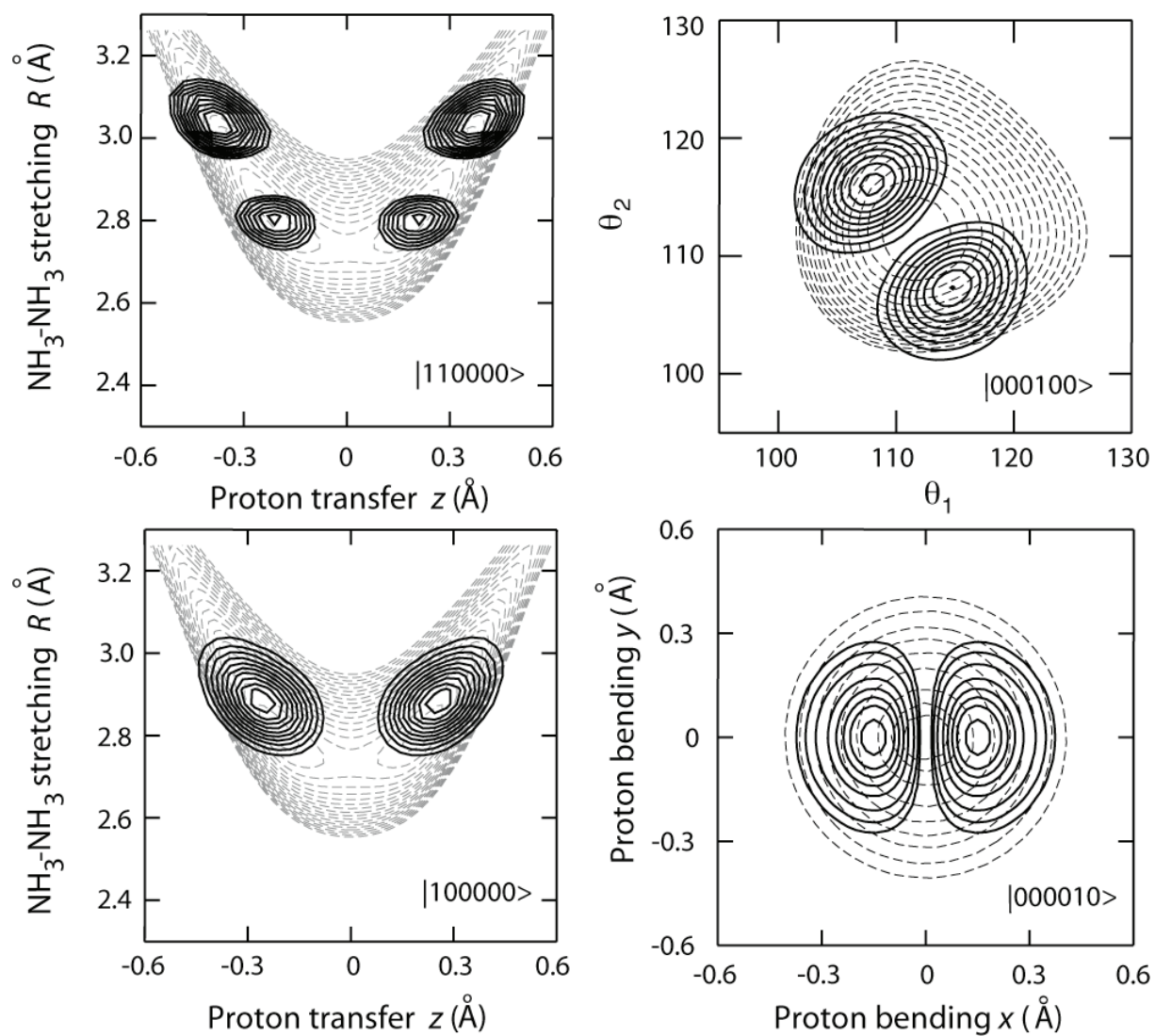
Yang et al.: Figure 1



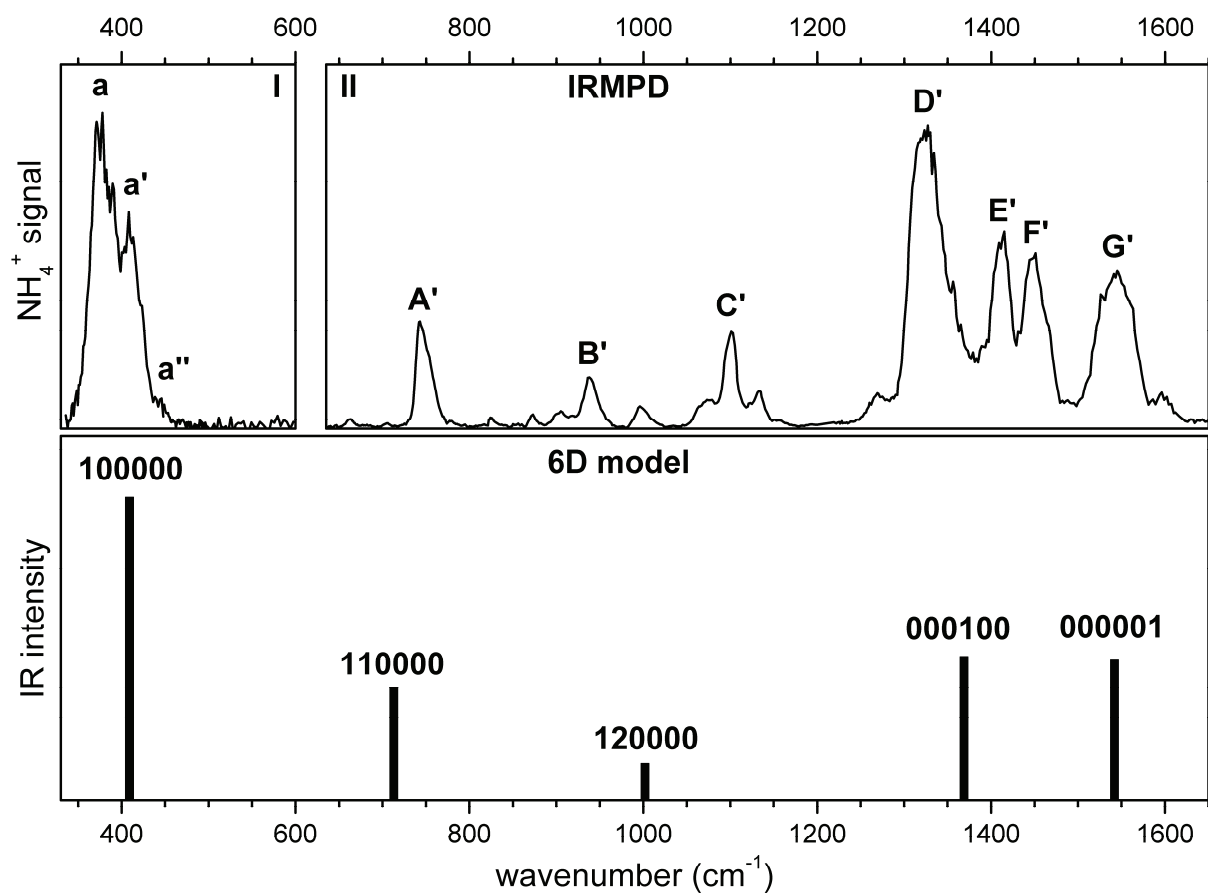
Yang et al.: Figure 2



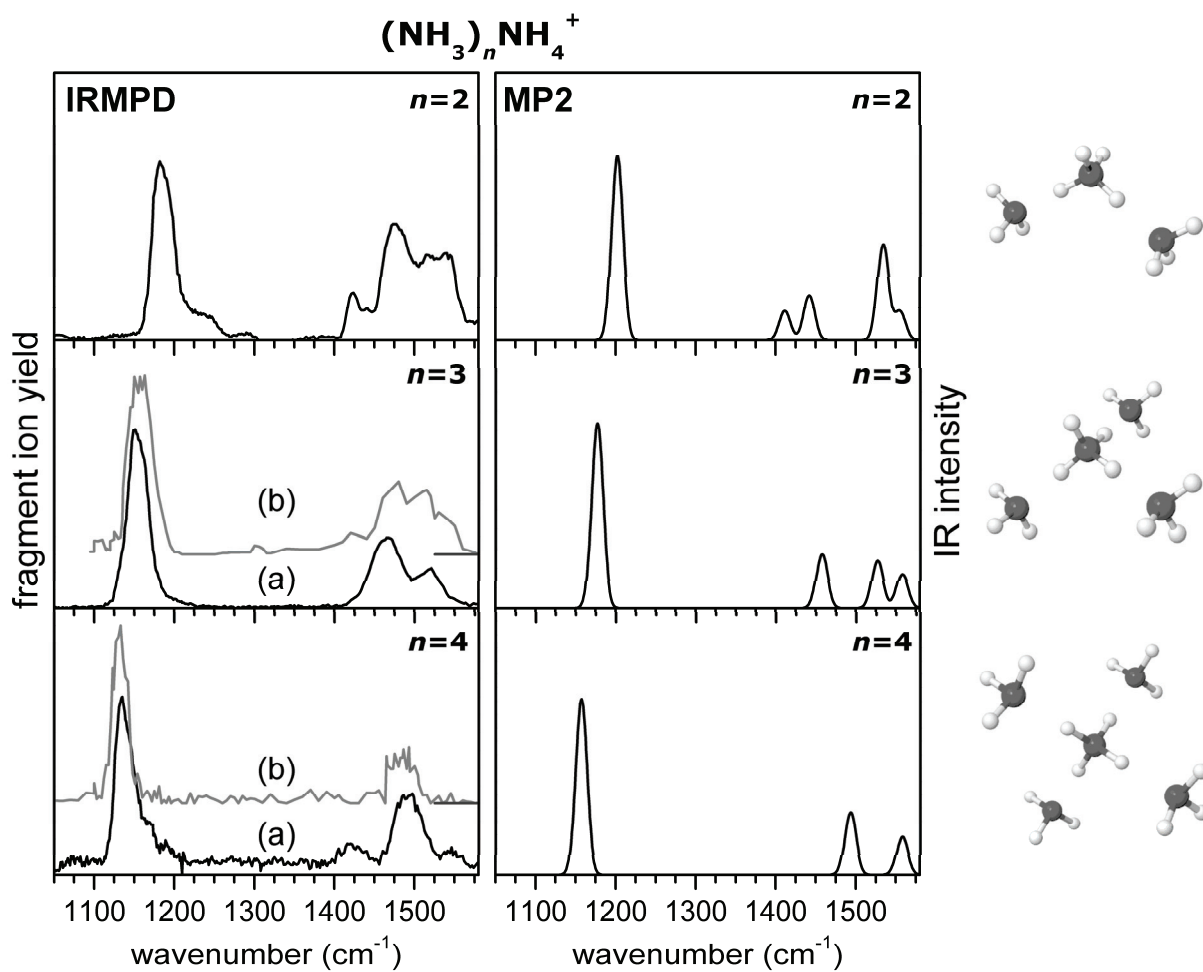
Yang et al.: Figure 3



Yang et al.: Figure 4



Yang et al.: Figure 5



Yang et al.: Figure 6